MODELING CARBON CHAIN ANIONS IN L1527

NANASE HARADA

Department of Physics, The Ohio State University, Columbus, OH 43210

AND

ERIC HERBST

Departments of Physics, Astronomy, and Chemistry, The Ohio State University, Columbus, OH 43210

ABSTRACT

The low-mass protostellar region L1527 is unusual because it contains observable abundances of unsaturated carbon-chain molecules including C_nH radicals, H_2C_n carbenes, cyanopolyynes, and the negative ions C_4H^- and C_6H^-, all of which are more associated with cold cores than with protostellar regions. Sakai et al. suggested that these molecules are formed in L1527 from the chemical precursor methane, which evaporates from the grains during the heat-up of the region. With the gas-phase osu.03.2008 network extended to include negative ions of the families C_n^-, and C_nH^-, as well as the newly detected C_3N^-, we modeled the chemistry that occurs following methane evaporation at $T \approx 25-30$ K. We are able to reproduce most of the observed molecular abundances in L1527 at a time of $\approx 5 \times 10^3$ yr. At later times, the overall abundance of anions become greater than that of electrons, which has an impact on many organic species and ions. The anion-to-neutral ratio in our calculation is in good agreement with observation for C_6H^-, but exceeds the observed ratio by more than 3 orders of magnitude for C_4H^-. In order to explain this difference, further investigation is needed on the rate coefficients for electron attachment and other reactions regarding anions.

Subject headings: astrochemistry — ISM: abundances — ISM: clouds — ISM: molecules

1. INTRODUCTION

L1527, an envelope of a low-mass star-forming region with IRAS 04368+2557 at its center, has the physical features of a class 0/I protostar, as discussed by André et al. (2000). The infalling collapse of circumstellar gas was observed by Ohashi et al. (1997) and the gas outflow was observed by Tamura et al. (1996). A number of interstellar molecules were discovered in L1527 as part of a molecular survey of dense cores by Jørgensen et al. (2004). Although one might expect the chemistry to be that of a hot corino (Ceccarelli et al. 2007), the temperature of the envelope is ≈ 30 K, well below that of hot corinos (100 K). More recently, Sakai et al. (2008b) detected unsaturated hydrocarbons and cyanopolyynes in the central core region of L1527. These species are unusual in corinos, and are more normally associated with cold ($T \approx 10$ K) dark clouds such as TMC-1 (Suzuki et al. 1992; Smith et al. 2004). Sakai et al. (2008b) explained the production of the carbon-chain species in terms of the evaporation of methane during the warm-up to 30 K followed by a rapid gas-phase synthetic chemistry, a process that they termed "warm carbon-chain chemistry." This chemistry is related to a grain mantle desorption model for TMC-1 of Markwick et al. (2000). In a recent paper, Hassel et al. (2008) used the Ohio State University (OSU) gas-grain code to study the warm-up chemistry of L1527 in the vicinity of 30 K and found that the carbon-chain abundances could be reasonably reproduced in this "lukewarm corino" by a chemistry in which gas-phase methane is the precursor. In addition to these unusual species, the two negative ion species C_6H^- and C_4H^- were also detected in L1527 (Sakai et al. 2007, 2008c; Agúndez et al. 2008).

Anions in the interstellar medium were first discussed by Dalgarno & McCray (1973). Herbst (1981) proposed that neutral radicals with large enough electron affinities can undergo efficient radiative attachment to form anions in cold dense clouds if they possess more than ≈ 4 atoms. Lepp & Dalgarno (1988) suggested that negatively charged polycyclic aromatic hydrocarbons (PAHs)

could also form by radiative attachment. Wakelam & Herbst (2008) modeled the gas-phase chemistry in dense cold cores with neutral and negatively charged PAHs, and found that the inclusion of PAHs allows good agreement with observations for small species with the use of so-called "high-metal" elemental abundances. Confirmation of anions in interstellar and circumstellar sources awaited the measurement of their rotational spectra in the laboratory by Thaddeus and coworkers (McCarthy et al. 2006; Gupta et al. 2007). In addition to the detections in L1527, C_6H^- and C_8H^- (McCarthy et al. 2006; Brünken et al. 2007) were detected in TMC-1, while C_4H^- (Cernicharo et al. 2007), C_6H^- (McCarthy et al. 2006; Kasai et al. 2007), and C_8H^- (Remijan et al. 2007) were observed in IRC+10216. In response to these detections, the anions C_n^-, $n = 5-10$, and C_nH^-, $n = 4-10$, were added to the RATE06[1] and IRC+10216 chemical networks (Millar et al. 2000) by Millar et al. (2007) with estimated or calculated rate coefficients (Terzieva & Herbst 2000) for radiative attachment and photodetachment processes as well as measured rate coefficients for associative detachment reactions. The augmented models were then used to study anionic abundances in TMC-1, IRC+10216, and photon-dominated regions such as the Horsehead Nebula. Millar et al. (2007) found that, as predicted earlier by Herbst (1981), hydrocarbon radical anions can reach abundances exceeding 1% of their neutral precursors, depending on their size. Another type of anion, C_3N^-, the radiative attachment of which was first studied by Petrie & Herbst (1997), was also detected recently in IRC+10216 by Thaddeus et al. (2008). Its radiative attachment rate coefficient has been calculated anew by Herbst & Osamura (2008), with a result similar to that of Petrie & Herbst (1997) used here.

In this paper, we restudy the gas-phase chemistry of L1527 with particular interest in the formation and depletion of anions and how their chemistry affects the overall chemistry of the

---

[1] See http://www.udfa.net.

TABLE 1
FORMATION AND DEPLETION REACTIONS FOR C_3N^-

Reaction	Rate Coefficient (cm^3 s^{-1})	Reference
$C_3N + e \rightarrow C_3N^- + h\nu$	$2.0 \times 10^{-10}(T/300)^{-0.5}$	1
$HNCCC + e \rightarrow C_3N^- + H$	$2.0 \times 10^{-8}(T/300)^{-0.5}$	2
$C_3N^- + H \rightarrow HC_3N + e$	1.0×10^{-9}	3
$C_3N^- + C \rightarrow C_4N + e$	1.0×10^{-9}	3
$C_3N^- + O \rightarrow C_2N + CO + e$	1.0×10^{-9}	3
$C_3N^- + h\nu \rightarrow C_3N + e$	$2.0 \times 10^{-9}\exp(-2.0A_v)$	4
$C_3N^- + C^+ \rightarrow C_3N + C$	$7.5 \times 10^{-8}(T/300)^{-0.5}$	5

REFERENCES.—(1) Petrie & Herbst 1997; (2) estimate based on Adams et al. 1986; (3) based on Eichelberger et al. 2007; (4) based on Millar et al. 2007; (5) sample positive ion; see Smith et al. (1978) for typical rates.

TABLE 2
INITIAL ABUNDANCES

Species	Fractional Abundance
C	1.0(−08)
O	1.0(−07)
Na	1.0(−11)
Si	3.0(−13)
CS	3.0(−09)
H_2	5.0(−01)
HCN	3.0(−09)
H_2O	1.0(−08)
N_2	1.0(−05)
O_2	1.0(−08)
He^+	1.0(−11)
S^+	1.0(−11)
Na^+	1.0(−11)
e^-	3.0(−09)
$(O)_{elem}$	5.0(−05)
He	6.0(−02)
Fe	1.0(−11)
S	1.0(−08)
CO	5.0(−05)
CH_4	3.0(−06)
CN	4.0(−09)
HNC	3.0(−09)
H_2S	1.0(−09)
NH_3	1.0(−08)
C^+	1.0(−09)
H_3^+	6.0(−11)
Fe^+	1.0(−11)
HCO^+	1.9(−09)
$(C)_{elem}$	5.3(−05)

NOTE.—The notation $a(-b)$ represents $a \times 10^{-b}$.

lukewarm corino. The osu.03.2008 gas-phase network[2] has been augmented to include formation and depletion reactions for the carbon cluster and hydrocarbon radical anions as well as for C_3N^-. The remainder of this paper is organized as follows. In § 2, we discuss the gas-phase code used and the choice of initial abundances. In § 3, the results are discussed and compared with observation for both anions and other species and with the earlier gas-grain results for non-anionic species. In § 4, we consider how our results respond to variations in initial abundances and to the exclusion of anionic chemistry. Finally, we end with a summary.

2. GAS-PHASE CODE AND INITIAL CONDITIONS

The recent OSU gas-phase network (see footnote 2) osu.03.2008 has been augmented by the addition of several families of negative ions and classes of reactions to form and destroy them. The new negative ions included in the model consist of the carbon chain families C_n^- ($n = 5–10$) and C_nH^- ($n = 4–10$) and the newly detected anion C_3N^-. The reaction classes include radiative attachment ($A + e \rightarrow A^- + h\nu$), photodetachment ($A^- + h\nu \rightarrow A + e$), dissociative attachment ($AB + e \rightarrow A^- + B$), associative detachment ($A^- + B \rightarrow AB + e$), anion-neutral reactions ($A^- + B \rightarrow C^- + D$), and mutual neutralization ($A^- + B^+ \rightarrow A + B$). Most of these classes of reactions are contained in the modified RATE06 network used in Millar et al. (2007). We have updated the rate coefficients for the radiative attachment of C_4H and C_5H according to the theory of Herbst & Osamura (2008). A large number of mutual neutralization reactions involving all anions and 57 major positive ions were added with rate coefficients $k = 7.5 \times 10^{-8}(T/300)^{-0.5}$ cm^3 s^{-1} (Smith et al. 1978; Wakelam & Herbst 2008); without these reactions, the correct balance of anions, electrons, and positive ions cannot be maintained for L1527 at later times, when the overall anionic abundance exceeds the electron abundance. Newly added reactions for the formation and depletion of C_3N^- and their rate coefficients are listed in Table 1. Overall, the augmented network for L1527 contains 5941 reactions involving 469 species, an extension of osu.03.2008, which contains 4479 reactions involving 468 species.

We follow the gas-phase chemistry after its warm-up from a cold cloud with icy mantles to a temperature in the range 25–30 K, by which most of the methane ice in grain mantles has evaporated along with other volatile species such as CO and N_2, which evaporate at slightly lower temperatures than methane. We use a temperature of 30 K, a total density $n_H = 10^6$ cm^{-3} and visual extinction $A_v = 10$ mag (Sakai et al. 2008b; Jørgensen et al. 2004). To convert observed column densities into fractional abundances,

we use a column density $N_H = 6 \times 10^{22}$ cm^{-2} (Jørgensen et al. 2004). The cosmic-ray ionization rate ζ is taken to be 1.3×10^{-17} s^{-1}. The initial abundances, shown in Table 2, are based on the gas-grain code results by Hassel et al. (2008), in which the gas and grain populations during the warm up are calculated. Since most of the water ice resides on grain mantles until much higher temperatures, the elemental carbon-to-oxygen abundance ratio in the gas is carbon-rich, as can be seen by adding up the carbon-containing and oxygen-containing species. The important precursor methane has a fractional abundance of 3×10^{-6}, in reasonable agreement with values obtained for cold ices using *Infrared Space Observatory* (*ISO*; Gibb et al. 2004) and *Spitzer* (Öberg et al. 2008). The low abundances for metals reflect the fact that most are still embedded in grain mantles. The chemistry starts quickly, as methane is partially converted into acetylene and more complex hydrocarbons via ion-molecule reactions (Hassel et al. 2008).

3. RESULTS

3.1. *Hydrocarbon Radicals and Anions*

Hydrocarbon radicals of the general linear structure C_nH are the main precursors to the C_nH^- anions through radiative attachment. The calculated fractional abundances (with respect to n_H) of C_4H, C_6H, C_8H, and $C_{10}H$ along with their respective anions as functions of time are shown in Figure 1. For the first 3×10^4 yr, the neutral radicals increase in abundance with abundances inversely proportional to size. At 10^3 yr, the main production channels of C_nH are dissociative recombination from precursor ions $C_nH_m^+$,

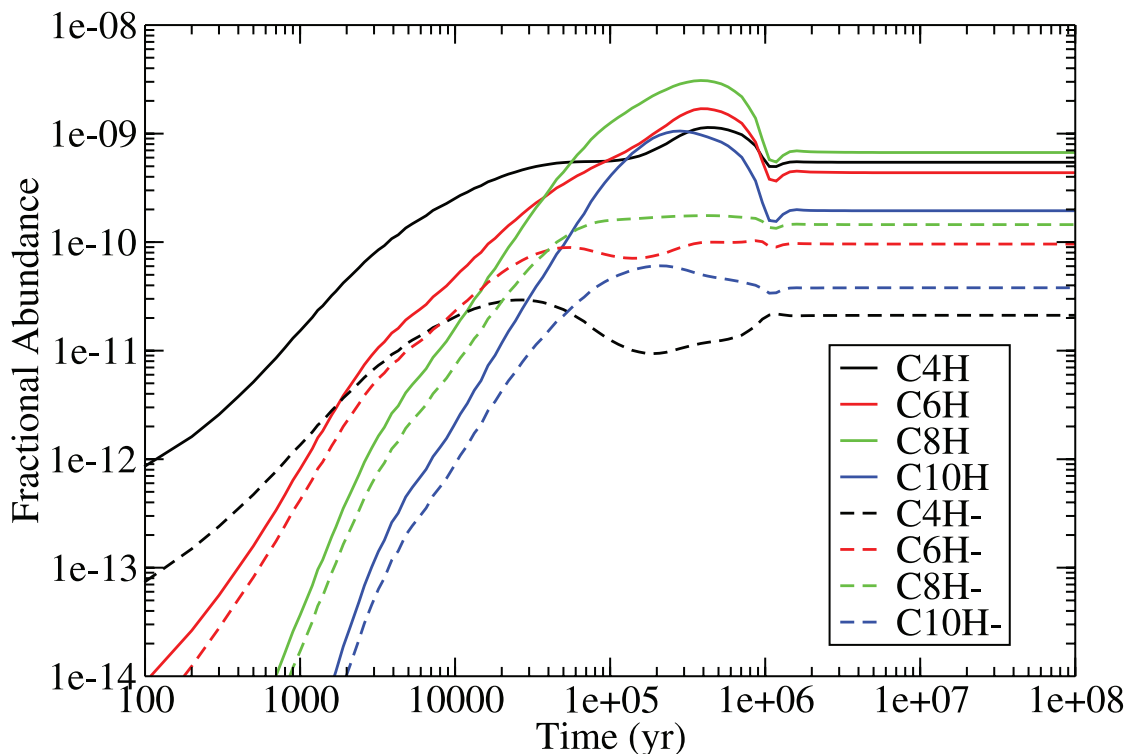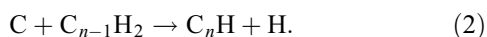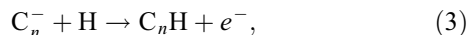$$C_nH_m^+ + e^- \rightarrow C_nH + \ldots, \qquad (1)$$
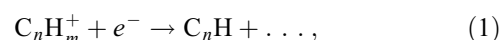
FIG. 1.—Fractional abundances with respect to n_H for $C_{2n}H$ and $C_{2n}H^-$ ($n = 2-5$) are plotted vs. time for our model of L1527.

and neutral-neutral reactions from smaller hydrocarbons,

$$C + C_{n-1}H_2 \rightarrow C_nH + H. \qquad (2)$$

The main formation reactions after 10^4 yr become the associative detachment processes

$$C_n^- + H \rightarrow C_nH + e^-, \qquad (3)$$

because the concentrations of the bare cluster anions become significant. When peak values are achieved, at a time of $\approx(3-5) \times 10^5$ yr, the size vs. fractional abundance order has broken down, and the most abundant radical becomes C_8H. The radical C_6H is next, while the still lower abundances of C_4H and $C_{10}H$ are similar. As steady state is achieved at still later times, the abundances of the three smallest radicals are nearly the same, while $C_{10}H$ is somewhat lower. The unusual dependence on size is due partially to carbon-rich elemental abundances and partially to the inclusion of anions, which increase the synthetic power of the chemistry and cause an "edge" effect, as discussed below in § 4.2.

The calculated fractional abundances of the C_nH anions, depicted in Figure 1, show an unusual dependence on size as well. At times after 4×10^4 yr, the most abundant anion is C_8H^-, which slightly exceeds the smaller C_6H^-. There is a gap in abundance between these two, and the pair of ions $C_{10}H^-$ and C_4H^-, which trail by a factor of 3–5. The relatively low concentration of C_4H^- is caused by the relative slowness of the radiative attachment reaction (Herbst & Osamura 2008),

$$C_4H + e^- \rightarrow C_4H^- + h\nu, \qquad (4)$$
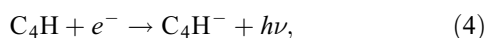
despite the fact that the calculated value of the rate coefficient is known to be too large (Herbst & Osamura 2008). The observed fractional abundances of C_4H^- and C_6H^- in L1527 are 1.8×10^{-13} and 9.7×10^{-13}, respectively (Sakai et al. 2007, 2008b). It

can be seen that while the calculated value for the larger anion is close to the observed value at relatively early times ($\approx 10^3$–10^4 yr), the calculated abundance for the smaller anion is far too large at all but the shortest times.

3.2. Cyanopolyynes and C_3N^-

Cyanopolyynes are produced via a variety of ion-molecule and neutral-neutral channels. The existence of the C_nH^- anions boosts the efficiency of one production mechanism,

$$CN + C_{2n}H_2 \rightarrow HC_{2n+1}N + H, \qquad (5)$$
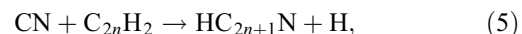
by enhancing the abundance of the precursor $C_{2n}H_2$ through the associative detachment reactions,

$$C_{2n}H^- + H \rightarrow C_{2n}H_2 + e^-. \qquad (6)$$
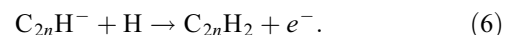
Although cyanoacetylene, HCCCN, can be formed by neutral-neutral channels, its higher energy isomers, such as HNCCC, are thought to be formed only through dissociative recombination (Osamura et al. 1999), viz.,

$$C_3H_2N^+ + e^- \rightarrow HNCCC + H. \qquad (7)$$

This particular isomer is important, because as can be seen in Table 1, it leads to the anion C_3N^- via an exothermic dissociative attachment reaction with hydrogen atoms. This synthesis can be competitive with the more simple radiative attachment depending on the source. Indeed, in L1527, it is the dominant pathway, as indicated in Figure 2, which shows the calculated fractional abundances of HC_3N, HNCCC, C_3N, and C_3N^- as functions of time. It can be seen that the abundance of the radical C_3N exceeds that of the isomer HNCCC for all times past 2×10^3 yr. However, the abundance of the radical does not exceed that of the isomer by more than a factor of 3, while the radiative attachment
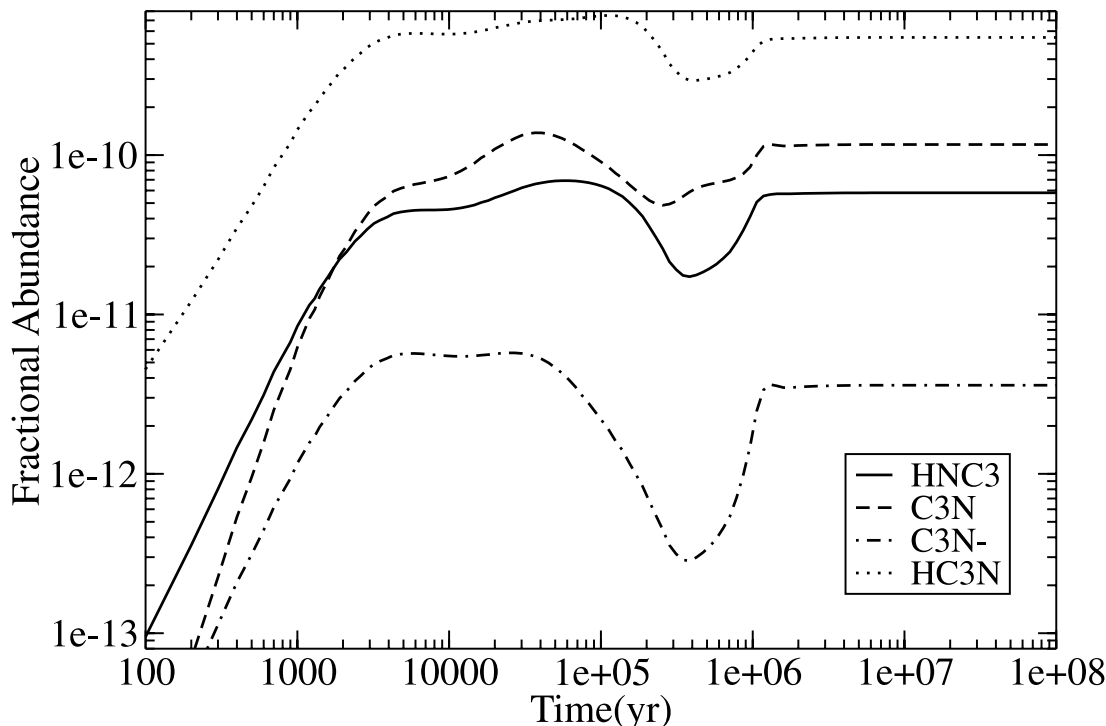
Fig. 2.—Calculated fractional abundances with respect to n_H for C_3N^-, HCCCN, HNCCC, and C_3N are plotted against time for L1527.

rate coefficient for $C_3N^- + e^-$ is lower than the dissociative attachment coefficient for $HNCCC + e^-$ by a factor of 100, as shown in Table 1. The predicted fractional abundance of the anion lies somewhere in the range 10^{-11} to 10^{-12} for most times. Although this range of values seems very low, it should be noted that the anion C_4H^- was detected with an even lower fractional abundance.

3.3. Anion-to-Neutral Ratio

The calculated and observed anion-to-neutral abundance ratios vs. time are shown in Figure 3 for C_4H and C_6H. Despite the fact that both anion and neutral are significantly overproduced at times $>10^4$ yr, the calculated C_6H^-/C_6H ratio always lies close to the observed value of $\approx 10\%$, exceeding it by at most a factor of 5 at early times, and dipping below by less than a factor of 2 before steady state is reached. This level of agreement suggests that the theoretical rate coefficient for the radiative attachment of C_6H (Herbst & Osamura 2008) is reasonably accurate, although the alternative possible formation route via dissociative attachment of the carbene H_2C_6 is not included in our network (Sakai et al. 2007; Herbst & Osamura 2008). The ratio C_4H^-/C_4H, as for other sources, is calculated to be much too large, due principally to the failure of the phase space treatment for the radiative attachment of C_4H (Herbst & Osamura 2008).

In Figure 4, we plot the fractional abundances of the electron, total positive ions, and total anions. After 4×10^4 yr, the total anion abundance exceeds the electron abundance, and anions become the dominant form of negatively charged particles. Since the mutual neutralizations of positive ions and negative ions are less rapid than dissociative recombination reactions between positive molecular ions and electrons, negative ions are likely to stay more abundant than electrons. Indeed, at steady state, the anionic abundance exceeds the electronic abundance by a factor of more than 2. Since anions can be more abundant than electrons, it was imperative to add a large number of mutual neutralization

reactions to make sure that the correct proportion of anion, electron, and positive ions was obtained.

3.4. Overall Comparison with Observation

To determine the best fit to the observed 23 abundances for the anions and other species in L1527, we used the mean confidence level method of Garrod et al. (2007). In this method, a confidence level κ_i is defined for each species i by the equation

$$\kappa_i = erfc\left(\frac{\left|\log(X_i) - \log(X_{\mathrm{obs},i})\right|}{\sqrt{2}\sigma}\right), \qquad (8)$$

where X_i is the computed fractional abundance, $X_{\mathrm{obs},i}$ the observed fractional abundance, and $\sigma = 1$. The agreement is perfect for $\kappa_i = 1$, a factor of 3 departure from observation if $\kappa_i = 0.63$, and a 1 order of magnitude departure from observation if $\kappa_i = 0.32$. We then take κ, the average value of κ_i, as the criterion for agreement. In our network of reactions, we do not make a distinction between the acetylenic forms HC_nH and the carbenes H_2C_n. Since only the latter are detected, we make the assumption that they represent only 1% of the total C_nH_2 abundance (Park et al. 2006). The optimal value of κ is 0.652 corresponding to an average agreement within a factor of 3; this agreement occurs at a time of 4.8×10^3 yr. The species and their observed and optimal calculated fractional abundance are shown in Table 3, where it can be seen that 18 of the 23 molecules have computed abundances within an order of magnitude of the observed values, while 15 have computed abundances within a factor of 3 of the observed values. The most extreme outlier is the anion C_4H^-, which is predicted to have an abundance higher than observed by a factor of 61. The other molecules that disagree with observation by more than an order of magnitude are C_4H, N_2H^+, and CN. Another anion, C_6H^-, is overproduced by an order of magnitude, and C_5H and HNC are overproduced by more than a factor of a few, while
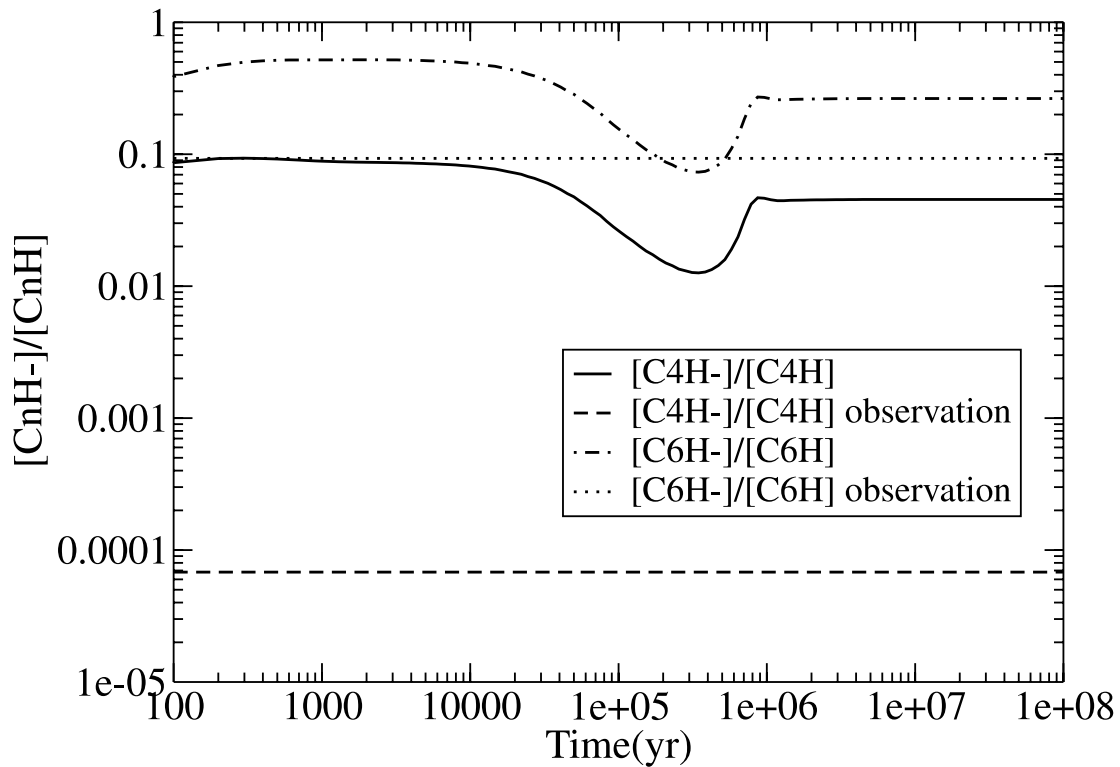
FIG. 3.—Calculated anion-to-neutral abundance ratio for C_4H and C_6H as a function of time. The observed values are plotted as horizontal lines.

HCO_2^+ is underproduced by factor of 5. The mean confidence limit is not a strong function of time, despite the fact that the abundances of carbon-chain molecules tend to keep increasing past the optimal time; at steady state, which occurs at times slightly in excess of 10^6 yr, the value of κ is still 0.474, corresponding to an average discrepancy factor of slightly more than

5. At steady state, 13 species are in agreement within an order of magnitude, and 9 of them are in agreement within a factor of 3. The main difference between the optimal time and steady state results concerns the abundances of carbon chain species, which become much larger than their observational values past the optimal time. In fact, at 5×10^5 yr, when these molecules achieve
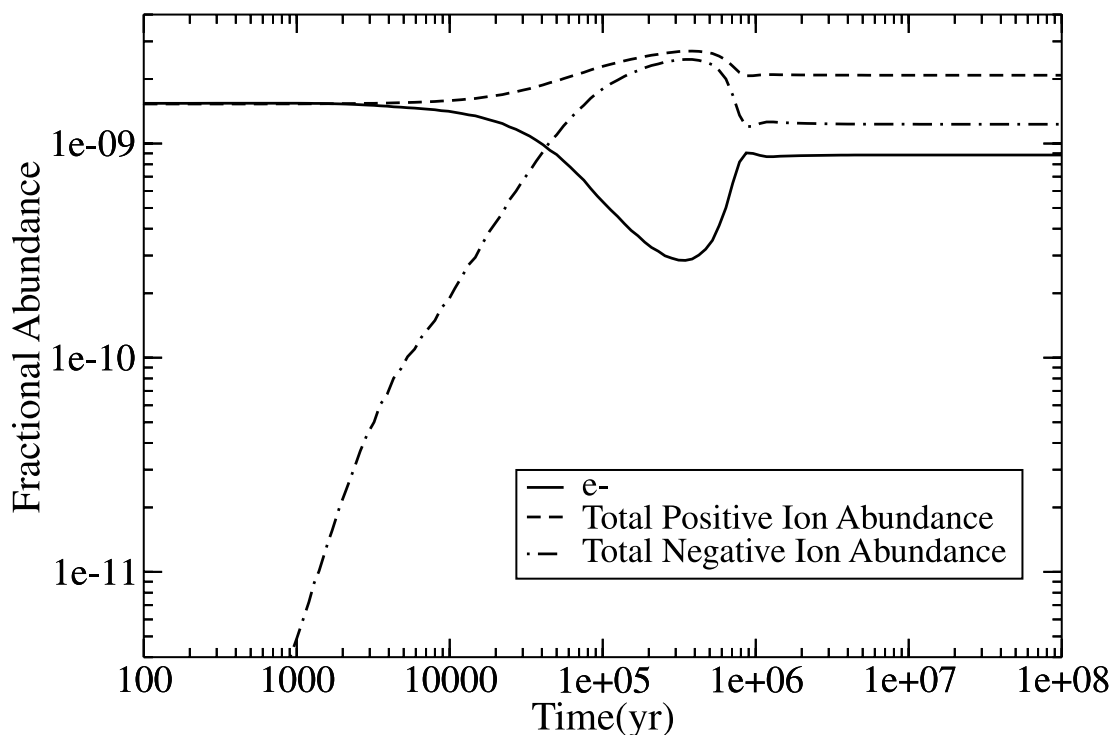

FIG. 4.—Calculated fractional abundances of electrons, the total positive ions, and the total negative ions are plotted against time. Note that the total negative ion abundance exceeds the electron abundance from a time of 3×10^4 yr.

TABLE 3
Observed and Optimal Calculated Abundances in L1527

Species	Observed Abundance	Reference	Calculated Abundance	Without Anions	Gas-Grain Model
CO....................	3.9(−05)	1	5.0(−5)	5.0(−5)	5.1(−05)
CN....................	8.0(−11)	1	1.4(−9)	1.1(−9)	9.6(−10)
CS....................	3.3(−10)	1	5.5(−10)	5.9(−10)	5.1(−09)
C$_2$S	8.5(−11)	2	1.6(−10)	1.7(−10)	1.3(−10)
HCN	1.2(−9)	1	1.3(−9)	1.3(−9)	7.7(−10)
HNC	3.2(−10)	1	1.5(−9)	1.4(−9)	6.3(−10)
SO	1.4(−10)	1	2.7(−10)	3.3(-10)	1.3(−10)
C$_4$H..................	3.3(−9)	2	1.3(−10)	5.7(−10)	1.7(−09)
C$_5$H..................	1.6(−11)	2	9.5(−11)	1.7(−10)	4.6(−10)
C$_6$H..................	1.0(−11)	2	1.9(−11)	4.8(−11)	2.3(−10)
C$_4$H$^-$	1.8(−13)	3	1.1(−11)	...	...
C$_6$H$^-$	9.7(−13)	4	9.8(−12)	...	...
HC$_3$N.................	8.9(−10)	1	5.5(−10)	5.8(−10)	4.0(−10)
HC$_5$N.................	9.7(−11)	2	1.1(−10)	1.4(−10)	1.6(−10)
HC$_7$N.................	2.7(−11)	2	1.4(−11)	1.8(−11)	2.9(−11)
HC$_9$N.................	2.5(−12)	2	2.1(−12)	2.3(−12)	5.9(−12)
H$_2$C$_3$	1.0(−11)	2	7.9(−12)	8.7(−12)	1.1(−11)
H$_2$C$_4$	2.2(−11)	2, 5	1.7(−11)	2.2(−11)	1.2(−10)
H$_2$C$_6$	2.5(−12)	2, 5	3.0(−12)	3.7(−12)	2.5(−11)
C$_3$H$_4$	7.8(−10)	2	1.4(−9)	1.7(−9)	2.2(−09)
HCO$^+$	6.0(−10)	1	1.3(−9)	1.2(−9)	1.7(−09)
N$_2$H$^+$	2.5(−10)	1	1.0(−11)	1.0(−11)	1.1(−11)
HCO$_2^+$	1.0(−12)	6	1.9(−13)	1.8(−13)	4.1(−13)

Note.—The notation $a(−b)$ represents $a \times 10^{−b}$.
References.—(1) Jørgensen et al. 2004; (2) Sakai et al. 2008b; (3) Agúndez et al. 2008; (4) Sakai et al. 2008c; (5) calculated carbene abundance was adjusted to 1% of total C$_n$H$_2$ (see § 3.4); (6) Sakai et al. 2008a.

their peak abundances, the confidence level is 0.411; a little worse than at steady state.

If we exclude the anions from our network, and fit for the remaining 21 molecular abundances in L1527, we find an optimal value for κ of 0.628 at 5.9×10^3 yr, corresponding to an average factor of 3 discrepancy, and a steady state value of 0.487, corresponding to an average factor of 5 discrepancy. The optimal results without anions are also tabulated in Table 3 as are the optimal results of the gas-grain warm-up model to 30 K (Hassel et al. 2008). This latter model, which does not contain anions, achieves an optimal agreement of a factor of 3 discrepancy when the temperature has risen to 25 K from its initial value of 10 K. The time spent up to 25 K when the gas-phase carbon chemistry can occur is roughly $(1−2) \times 10^4$ yr. Comparison of the gas-phase models with the gas-grain model shows that the gas-phase model without anions achieves somewhat closer agreement with the gas-grain model, because, as discussed later, the anions do affect the chemistry. It should also be noted that the observed molecular abundances toward L1527 excluding anions can also be fit to within an order of magnitude by a cold model, especially the non–carbon-chain species, which may not be spatially correlated with the carbon-chain molecules (Hassel et al. 2008).

Predicted abundances for a wide class of molecules using the optimal times of the gas-phase fit with anions as well as the gas-grain warm-up model to 30 K are listed in Table 4. Most optimum gas-phase abundances tend to be only slightly smaller than their gas-grain counterparts. Other than the negative ions, some significant disagreements (>1 order of magnitude) concern the hydrocarbon radicals, which are depleted by electron attachment in the gas-phase model, the carbenes, and species such as methanol, which are not produced efficiently in the gas phase. Despite the fact that the gas-grain prediction for methanol is much

higher than the gas-phase result, methanol is still predicted to be of very low abundance in the gas until the temperature warms up to hot core levels (Hassel et al. 2008).

4. RESPONSE TO VARIATIONS

4.1. Varying Initial Conditions: Oxygen and Methane

Unlike the gas-grain approach of Hassel et al. (2008) to L1527, where the evaporation of the volatile mantle species is determined by the chemical and physical processes, in the gas-phase approach we can vary the initial abundances from those listed in Table 2, which derive from evaporation from grain mantles in the warm-up gas-grain model. It is useful to be able to vary the initial abundances because the warm-up scenario is approximate at best. Here we consider variations in the initial abundances of atomic oxygen and methane (CH$_4$). The C/O elemental abundance ratio is 1.06 with our standard abundances; an increase in O will move the ratio closer to unity. The amount of methane is important to the warm carbon chemistry, since it is the precursor for all of it, and since its observed prior abundance in ices can vary (Öberg et al. 2008).

Table 5 shows the effect of changing the initial abundance of atomic oxygen on the time of best agreement, the average confidence level κ, and the number of species within order-of-magnitude agreement with observation. Although the O abundance is not large, O atoms tend to destroy organic ions and radicals. Varying the fractional O abundance from $5 \times 10^{−8}$ to $1 \times 10^{−6}$ shows that the optimal value for κ peaks for $(1−2) \times 10^{−7}$, although the criterion of number of molecules fitted to within an order of magnitude peaks at $5 \times 10^{−7}$. The sensitivity to changes in O abundance, however, is minimal. On the other hand, the time of best agreement increases with increasing initial abundance of O. This latter dependence arises from the fact that O slows down the synthetic process.

TABLE 4

PREDICTED OPTIMAL FRACTIONAL ABUNDANCES
OF UNOBSERVED GASEOUS SPECIES

Species	Gas-Phase Model	Gas-Grain Model
C_3H	3.3(−10)	1.0(−9)
C_7H	4.4(−12)	1.3(−10)
C_8H	4.1(−12)	1.1(−10)
C_9H	8.3(−13)	7.2(−11)
$C_{10}H$	4.5(−13)	...
C_5H^-	3.0(−11)	...
C_7H^-	7.2(−12)	...
C_8H^-	1.9(−12)	...
C_9H^-	1.2(−12)	...
$C_{10}H^-$	2.0(−13)	...
CH_4	2.9(−6)	3.9(−6)
C_2H_2	1.4(−8)	3.7(−8)
H_2C_5	8.0(−12)	2.5(−11)
H_2C_7	1.4(−12)	7.1(−12)
H_2C_8	5.8(−13)	5.6(−12)
H_2C_9	2.6(−13)	2.6(−12)
CH_3C_4H	2.0(−10)	1.1(−9)
CH_3C_6H	1.4(−11)	1.7(−10)
$HC_{11}N$	1.1(−13)	...
$HC_{13}N$	5.2(−15)	...
C_2N	2.2(−10)	4.3(−10)
C_3N	6.0(−11)	1.2(−10)
C_4N	4.3(−11)	1.7(−10)
C_5N	8.6(−11)	1.4(−10)
C_7N	1.0(−11)	2.6(−11)
C_9N	1.3(−12)	5.1(−12)
CH_3C_3N	1.5(−13)	2.9(−13)
CH_3C_5N	7.5(−15)	2.3(−14)
CH_3C_7N	8.2(−16)	3.8(−15)
C_3N^-	5.5(−12)	...
N_2	1.0(−5)	5.6(−6)
O_2	7.4(−9)	1.1(−8)
H_2O	7.4(−10)	8.8(−10)
NH_3	7.0(−9)	3.7(−9)
CO_2	2.2(−9)	4.1(−9)
He^+	1.9(−12)	8.8(−12)
C^+	2.9(−11)	1.1(−10)
HCO^+	1.3(−9)	1.7(−9)
H_3^+	2.7(−11)	5.6(−11)
H_3O^+	8.8(−12)	1.3(−11)
$c-C_3H_2$	4.2(−10)	5.7(−10)
C_6H_6	6.5(−11)	3.2(−10)
CH_2CN	4.4(−11)	7.4(−11)
H_2CO	5.4(−9)	4.3(−9)
$HCOOH$	3.1(−12)	3.6(−12)
CH_2CO	1.2(−9)	1.0(−9)
CH_3CN	2.8(−12)	2.0(−12)
CH_3OH	3.4(−16)	5.0(−11)
$HCOOCH_3$	1.8(−19)	3.8(−15)
CH_3OCH_3	2.3(−17)	3.8(−16)
H_2CS	1.2(−9)	5.2(−10)
H_2S	7.7(−10)	3.3(−9)

NOTE.—The notation $a(−b)$ represents $a \times 10^{−b}$.

Regarding methane, the results for time of best agreement, κ, and order-of-magnitude agreement are shown in Table 6. There is little dependence on the optimal fit defined by either the κ criterion or the number-of-molecules criterion as the initial methane abundance is raised from $3 \times 10^{−7}$ to $3 \times 10^{−5}$. Here, however, the time of optimal agreement decreases with increasing methane abundance. Presumably the higher abundance of methane leads to the more rapid production of carbon-chain species.

TABLE 5

DEPENDENCE OF AGREEMENT WITH OBSERVATION
ON THE ATOMIC OXYGEN ABUNDANCE

Initial Fractional Oxygen Abundance	κ	Time of Best Agreement (yr)	Number of Species in Agreement
5.0(−08)	0.649	4.3(03)	18
1.0(−07)	0.652	4.8(03)	18
2.0(−07)	0.652	5.9(03)	19
5.0(−07)	0.636	7.2(03)	20
1.0(−06)	0.621	8.0(03)	18

NOTE.—The notation $a(−b)$ represents $a \times 10^{−b}$.

4.2. The Effect of Anions

It is interesting to compare the chemistry of our gas-phase model for L1527 with and without anions in more detail. Given that the overall abundance of anions in the model exceeds that of electrons at times later than 4×10^4 yr, one would expect the effect of anions to be more pronounced at such times. By and large, this inference is true although for some classes of molecules there is little effect at all at earlier times, while for other species the effect is already a large one. In Figure 5, we plot the fractional abundances of four classes of molecules vs. time—the $C_{2n}H$ radicals (*top left panel*), the hydrocarbons C_nH_2, consisting mainly of polyynes ($HC_{2n}H$) with small abundances of carbenes H_2C_{2n} (*top right panel*), the bare carbon clusters (*bottom left panel*), and the cyanopolyynes $HC_{2n+1}N$ (*bottom right panel*)—with and without anionic chemistry. Let us start with the hydrocarbons. Here it can be seen that the effect caused by the anions increases with time, as expected, so that by steady state the abundances computed without anions are mainly significantly lower than those computed with anions. The reason is that the C_nH anions increase the abundances of the hydrocarbons via reaction (6) as well as the analogous processes for odd numbers of carbon atoms. We also note that at later times, including steady state, the largest hydrocarbon depicted, C_8H_2, has the largest abundance in the model with anions, and the smallest abundance in the model without anions. The chemistry leading to this unusual result is complex and will be the subject of a future paper. For now, we note only that the existence of anions has a catalytic effect on the production of more complex hydrocarbons from simpler ones. For example, starting with the hydrocarbon C_6H_2, reaction with carbon atoms leads to the species C_7H (see reaction [2]), which is efficiently converted to its anion. The anion, in turn, undergoes an associative detachment reaction with atomic hydrogen to form the more complex hydrocarbon C_7H_2 (see reaction [3]). The process continues through the largest hydrocarbon in the model. The enhanced abundance of this largest hydrocarbon suggests that still larger species must be included in the model to avoid an "edge" effect for potentially observable species, in which

TABLE 6

DEPENDENCE OF AGREEMENT WITH OBSERVATION ON THE METHANE ABUNDANCE

Initial Fractional Methane Abundance	κ	Time of Best Agreement (yr)	Number of Species in Agreement
3.0(−07)	0.601	8.8(03)	18
1.0(−06)	0.642	6.5(03)	18
3.0(−06)	0.652	4.8(03)	18
1.0(−05)	0.652	4.3(03)	19
3.0(−05)	0.647	4.3(03)	19

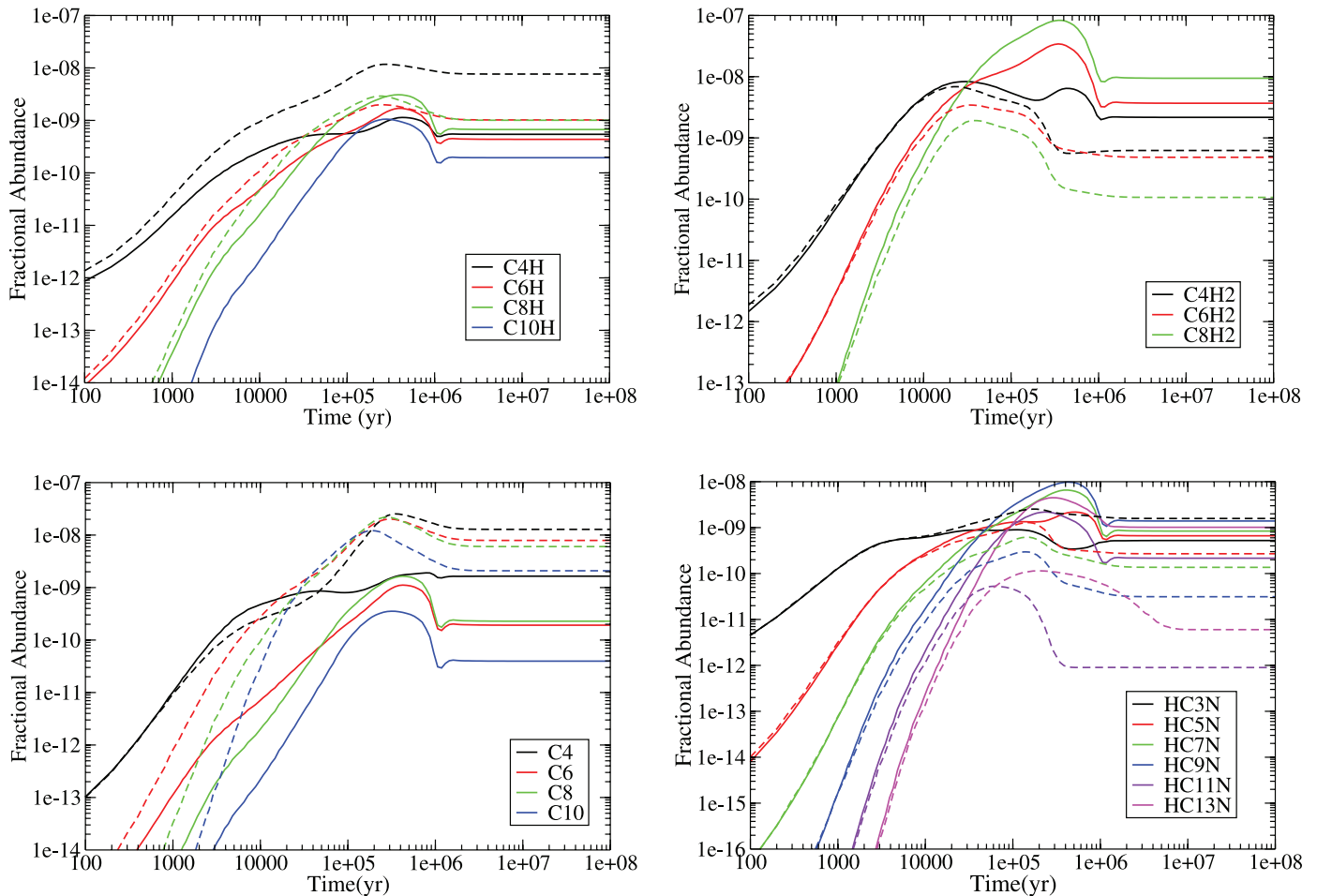NOTE.—The notation $a(−b)$ represents $a \times 10^{−b}$.

Fig. 5.—Comparison of the time-dependent abundances of selected families of molecules — hydrocarbon radicals ($C_{2n}H$; *top left*), hydrocarbons ($C_{2n}H_2$; *top right*), carbon clusters (C_{2n}; *bottom left*), and cyanopolyynes ($HC_{2n+1}N$; *bottom right*) — with and without negative ions. Solid lines show the results with negative ions, while dotted lines show the results without negative ions. Note that $C_{10}H$ is not included in the network without anions.

the concentrations of the larger species are overestimated due to a paucity of destruction reactions.

If we look at the cyanopolyynes the result, although more complex, is similar to that of the hydrocarbons. The enhanced synthetic power with anions is doubtless caused by the enhanced production of these hydrocarbons, which can react with the radical CN to produce cyanopolyynes, as shown in reaction (5). The late-time abundance of the largest cyanopolyyne shown, $HC_{13}N$, is comparable with those of smaller cyanopolyynes. On the other hand, the plot of the $C_{2n}H$ radicals shows that the existence of anions decreases their abundances starting at rather early times. This effect is surprising because bare carbon anions are eventually involved in their formation (see reaction [3]), but presumably destruction via the formation of anions is more important. For the bare carbon clusters, destruction by the formation of anions causes a similar effect.

5. SUMMARY

L1527 is an unusual source because the unsaturated carbon-chain molecules detected there are more normally associated with cold dense cores at lower temperatures. Sakai et al. (2008b) proposed that the carbon-chain chemistry starts soon after rising temperatures allow the volatile species methane to evaporate into the gas. Our group has studied this chemistry via two types of models. In a previous model, Hassel et al. (2008) used the OSU gas-grain code to study the chemistry in a cold dense core followed

by warm-up to temperatures associated with L1527 ($T \approx 30$ K) and found a rich chemistry leading to carbon-chain species, as hypothesized by Sakai et al. (2008b). Comparison with observation showed that although the non–carbon-chain species in L1527 could be fit well either as remnants of a previous cold phase or current denizens of the warm-up phase, the carbon-chain species are fit significantly better with the warm model. Although the gas-grain approach was quite useful, this method does not contain any anionic chemistry, and the chemistry is fixed by what happens in the earlier cold epoch and the rising temperatures. We have followed this prior study with the isothermal ($T = 30$ K) gas-phase study reported here because it allows us to include the gas-phase anionic chemistry without worrying about what happens when anions collide with grains, and because it allows us to vary some of the initial abundances, which are mainly based on the earlier model. The abundance of methane, for example, has been studied in the ice phase of cold sources (Öberg et al. 2008) prior to evaporation and found to depend somewhat on the source investigated.

Including the chemistry of carbon-chain anions in our gas-phase network has led to a large increase in the number of reactions, mainly because of the many cation-anion neutralization reactions needed. With the chosen initial abundances, the best agreement with all 23 observed molecules in L1527 occurs at a time of 4.8×10^3 yr, when the abundances of most carbon-chain species are increasing. This agreement corresponds to an average factor of 3 discrepancy between observational and calculated values.

Variation in the initial abundances of either atomic oxygen or methane changes the time of best agreement mainly because these species regulate both the formation and depletion rates of carbon-chain species. For the observed anions, C_4H^- and C_6H^-, we fit both the fractional abundance and the anion-to-neutral ratio reasonably well for the larger anion, but dramatically overproduce these quantities for the smaller anion. Finally, it is to be noted that the steady state abundances in the gas-phase model are reached by 10^6 yr, so that the chemical processes of interest in this paper are completed well before the gas-grain models show declines in the gas-phase abundances (Hassel et al. 2008).

A comparison of the chemistry occurring with and without negative ions shows that anions have a major effect on the chemistry of other species, especially at later times than that for the optimal fit, when the overall anionic abundance exceeds that of electrons. This effect can either lower abundances of a given class of molecules or raise them, depending on whether the formation of anions tends to deplete other species or enhance their production. There is also a strange effect in which the dependence of the abundance of a molecule in a family, such as the cyanopolyynes, on size is changed when anions are included in the chemistry. Typically, in the absence of anions, an increase in size results in a drop in peak abundance. The inclusion of anions appears to make this dependence significantly smaller and even to vitiate it completely in some instances. As will be shown in subsequent work, this effect is also pronounced in the cold core TMC-1 under oxygen-rich conditions. With relatively large abundances for the largest carbon-containing species in our network, it may well be necessary to add still larger molecules to the model, either by including all of the formation and depletion reactions that govern their chemistry, as in the IRC+10216 network (Millar et al. 2000), or by some more approximate approach (Herbst 1991). In addition, despite the size of the current network, the role of negative ion-neutral reactions remains to be fully explored (Cordiner et al. 2008; M. A. Cordiner & T. J. Millar 2008, in preparation).

REFERENCES

Adams, N. G., Smith, D., Viggiano, A. A., Paulson, J. F., & Henchman, M. J. 1986, J. Chem. Phys., 84, 6728
Agúndez, M., Cernicharo, J., Guélin, M., Gerin, M., McCarthy, M. C., & Thaddeus, P. 2008, A&A, 478, L19
André, P., Ward-Thompson, D., & Barsony, M. 2000, in Protostars and Planets IV, ed. V. Mannings, A. P. Boss, & S. S. Russell (Tucson: Univ. Arizona Press), 59
Brünken, S., Gupta, H., Gottlieb, C. A., McCarthy, M. C., & Thaddeus, P. 2007, ApJ, 664, L43
Ceccarelli, C., Caselli, P., Herbst, E., Tielens, A. G. G. M., & Caux, E. 2007, in Protostars and Planets V, ed. B. Repurth, D. Jewitt, & K. Keil (Tucson: Univ. Arizona Press), 47
Cernicharo, J., Guélin, M., Agúdez, M., Kawaguchi, K., McCarthy, M. C., & Thaddeus, P. 2007, A&A, 467, L37
Cordiner, M. A., Millar, T. J., Walsh, C., Lis, D., Bell, T., Roueff, E., & Herbst, E. 2008, in Proc. IAU Symp. 251, Organic Matter in Space, ed. S. Kwok & S. A. Sanford (Cambridge: Cambridge Univ. Press), in press
Dalgarno, A., & McCray, R. A. 1973, ApJ, 181, 95
Eichelberger, B., Snow, T. P., Barckholtz, C., & Bierbaum, V. M. 2007, ApJ, 667, 1283
Garrod, R., Wakelam, V., & Herbst, E. 2007, A&A, 467, 1103
Gibb, E. L., Whittet, D. C. B., Boogert, A. C. A., & Tielens, A. G. G. M. 2004, ApJS, 151, 35
Gupta, H., Brünken, S., Tamassia, F., Gottlieb, C. A., McCarthy, M. C., & Thaddeus, P. 2007, ApJ, 655, L57
Hassel, G. E., Herbst, E., & Garrod, R. T. 2008, ApJ, 681, 1385
Herbst, E. 1981, Nature, 289, 656
———. 1991, ApJ, 366, 133
Herbst, E., & Osamura, Y. 2008, ApJ, 679, 1670
Jørgensen, J. K., Schöier, F. L., & van Dishoeck, E. F. 2004, A&A, 416, 603

Kasai, Y., Kagi, E., & Kawaguchi, K. 2007, ApJ, 661, L61
Lepp, S., & Dalgarno, A. 1988, ApJ, 324, 553
Markwick, A. J., Millar, T. J., & Charnley, S. B. 2000, ApJ, 535, 256
McCarthy, M. C., Gottlieb, C. A., Gupta, H., & Thaddeus, P. 2006, ApJ, 652, L141
Millar, T. J., Herbst, E., & Bettens, R. P. A. 2000, MNRAS, 316, 195
Millar, T. J., Walsh, C., Cordiner, M. A., Chuimín, R. Ní, & Herbst, E. 2007, ApJ, 662, L87
Öberg, K. I., Boogert, A. C. A., Pontoppidan, K. M., Blake, G. A., Evans, N. J., Lahuis, F., & van Dishoeck, E. F. 2008, ApJ, 678, 1032
Ohashi, N., Hayashi, M., Ho, P. T. P., & Momose, M. 1997, ApJ, 475, 211
Osamura, Y., Fukuzawa, K., Terzieva, R., & Herbst, E. 1999, ApJ, 519, 697
Park, I. H., Wakelam, V., & Herbst, E. 2006, A&A, 449, 631
Petrie, S., & Herbst, E. 1997, ApJ, 491, 210
Remijan, A., Hollis, J. M., Lovas, F. J., Cordiner, M. A., Millar, T. J., Markwick-Kemper, A. J., & Jewell, P. R. 2007, ApJ, 664, L47
Sakai, N., Sakai, T., Aikawa, Y., & Yamamoto, S. 2008a, ApJ, 675, L89
Sakai, N., Sakai, T., Hirota, T., & Yamamoto, S. 2008b, ApJ, 672, 371
Sakai, N., Sakai, T., Osamura, Y., & Yamamoto, S. 2007, ApJ, 667, L65
Sakai, N., Sakai, T., & Yamamoto, S. 2008c, ApJ, 673, L71
Smith, D., Church, M. J., & Miller, T. M. 1978, J. Chem. Phys., 68, 1224
Smith, I. W. M., Herbst, E., & Chang, Q. 2004, MNRAS, 350, 323
Suzuki, H., Yamamoto, S., Ohishi, M., Kaifu, N., Ishikawa, S., Hirahara, Y., & Takano, S. 1992, ApJ, 392, 551
Tamura, M., Ohashi, N., Hirano, N., Itoh, Y., & Moriarty-Schieven, G. H. 1996, AJ, 112, 2076
Terzieva, R., & Herbst, E. 2000, Int. J. Mass Spectrom., 201, 135
Thaddeus, P., Gottlieb, C. A., Gupta, H., Bruënken, S., McCarthy, M. C., Agúndez, M., Guélin, M., & Cernicharo, J. 2008, ApJ, 678, 1032
Wakelam, V., & Herbst, E. 2008, ApJ, 680, 371